Supplement of Hydrol. Earth Syst. Sci., 29, 4281–4305, 2025
https://doi.org/10.5194/hess-29-4281-2025-supplement

Hydrology and Earth System Sciences
Open Access
EGU

Supplement of

Topothermohaline convection – from synthetic simulations to reveal processes in a thick geothermal system

Attila Galsa et al.

Correspondence to: Ádám Tóth (a.z.toth@uu.nl)

S1 Water density and molecular diffusion

In the synthetic and real case simulations, water density depended on the temperature, pressure and salt concentration as a sixth-order polynomial, a second-order polynomial and a linear function, respectively, following the formula of

$$\varrho_w(T,p,c) = \sum_{j=0}^{6}\sum_{i=0}^{2} a_{ij}p^iT^j + a_{00}\beta c, \quad \text{(S1)}$$

where the first term provides the temperature- and pressure-dependent water density with an accuracy of 0.5% for a range of $p_{sat}<p\leq100$ MPa and $0\leq T\leq350$ °C (Magri, 2009), and the second term is the linear effect of concentration on water density (Kohfahl et al., 2015). Coefficients for a_{ij} are reported in Magri (2009), while $\beta=7.1\cdot10^{-4}$ l g^{-1} was used after Kohfahl et al. (2015).

A quadratic form of Arrhenius law was applied to calculate the temperature-dependent molecular diffusion coefficient,

$$D_{diff}(T) = D_0\exp\left[\frac{A}{T^2}+\frac{B}{T}+C\right], \quad \text{(S2)}$$

where $D_0=10^{-9}$ m^2 s^{-1}, temperature is given in K, constants of A=-352 450.2 K^2, B=163.6348 K and C=4.247125 were determined by fitting on data of Easteal et al. (1989) with an error of less than 0.02%.

S2 Effect of mechanical dispersion in synthetic models

Mechanical dispersivity in synthetic models was neglected ($\alpha_L=\alpha_T=0$) to focus on the dynamic interaction between topography-driven forced and free thermohaline convection. Here, an additional model is presented, in which α_L=100 m and α_T=10 m were applied in the base model (H=50 m, q_{Tb}=90 mW m^{-2}, c_b=70 g l^{-1}) to capture the effect of dispersion. Quasi-stationary solution after 3 Myr is presented in Figure S1 showing that a more extensive thermohaline dome developed beneath the discharge zone (left) compared to the base model (Fig. 2) due to the facts that (1) the transverse dispersion increased concentration flux through the bottom boundary, and (2) the longitudinal dispersion effectively mixed the groundwaters in the basin. The phenomenon is very similar to the behaviour of the saltwater zones in synthetic topohaline convection models, where the effect of dispersivity was investigated in detail (Galsa et al., 2022). The relative area of the saline water zone increased from A_{sal}=35% to 50% resulting in higher average concentration (from c_{av}=12.2 g l^{-1} to 27.1 g l^{-1}), temperature (from T_{av}=34.7 °C to 45.8 °C) and water age (from τ_{av}=121 kyr to 170 kyr) as well as lower Darcy flux (from $q_{av}=4.79\cdot10^{-9}$ m s^{-1} to 4.20 m s^{-1}). Thus, mechanical dispersion, like other physical/numerical parameters (e.g. temperature- and pressure-dependent viscosity, boundary conditions), strongly influences the behaviour of the complex system.

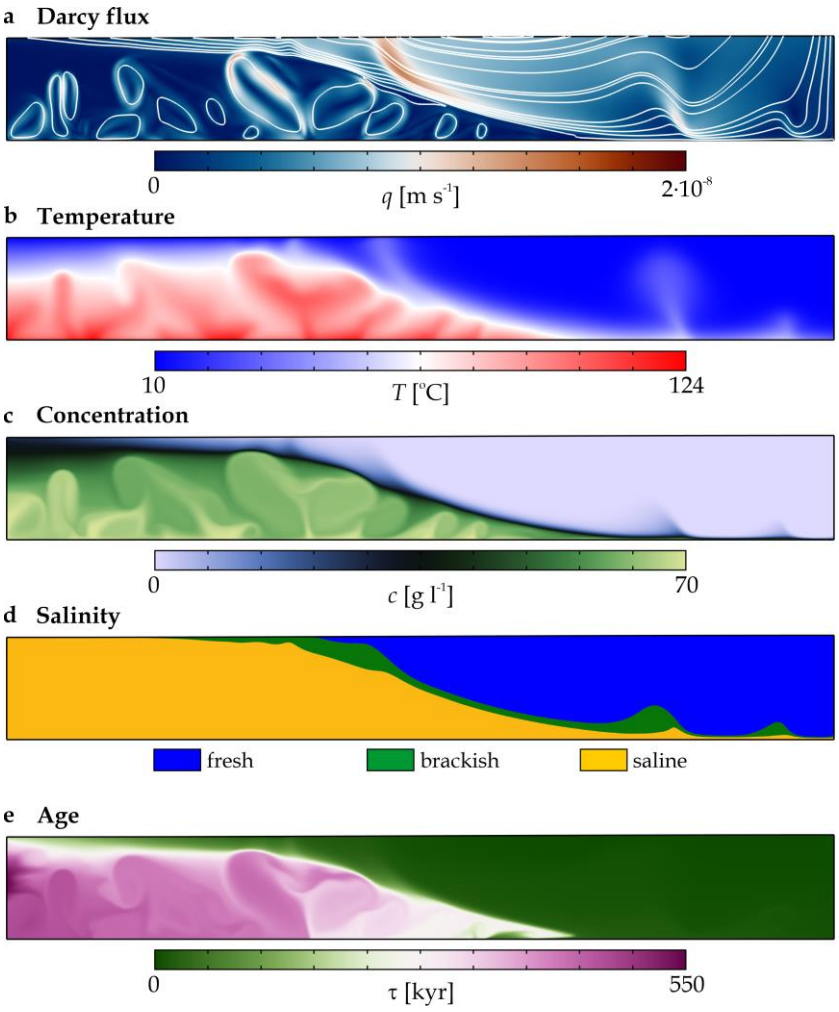

Figure S1 Snapshots of the (a) Darcy flux, (b) temperature, (c) salt concentration, (d) salinity zones and (e) groundwater mean age at t=3 Myr after the initial state in the base model (Table 2) including longitudinal (α_L=100 m) and transverse (α_T=10 m) dispersivity. (a) Streamlines illustrate the flow direction. (d) Salinity zones: freshwater (blue), brackish water (green) and saline water (orange).

S3 Effect of the side wall on the thermohaline dome

Undoubtedly, all boundary conditions affect the numerical solution obtained in the model domain, whether it is a synthetic or real model, whether it refers to flow, temperature, salt concentration or water age. If a thermohaline dome is formed in a synthetic model, it always develops beneath the discharge zone, near the vertical no-flow (Darcy flux), thermally insulating (temperature) and no-flux (salt concentration and water age) boundary. Therefore, the qualitative and quantitative impact of the lateral boundary on the topothermohaline system evolving in the synthetic model was investigated, and in particular on the thermohaline dome. In order to eliminate the side boundary effect, two sinusoidal unit basins were merged with the parameters

of the base model (Table 2), in which the discharge zone was located in the middle of the domain and thus unaffected by the side boundaries and boundary conditions.

The thermohaline dome also formed under these conditions (unaffected by lateral boundaries), so it is clear that the dome beneath the discharge zone is the hydro-geophysical consequence of the system, and not an artificial phenomenon caused by the vertical boundary condition (Fig. S2). The thermohaline dome developed in the doubled model domain is now dynamically bounded on both sides, and intense thermohaline convection occurs within it. Comparing its quantitative characteristics with the base model, it was found that the relative size of the thermohaline dome decreased from A_{sal}=35% to 31%, and its average Darcy flux was essentially unchanged (from q_{sal}=2.64·10^{-9} m s^{-1} to 2.76·10^{-9} m s^{-1}), its temperature, salt concentration and age decreased from T_{sal}=62.9 °C, c_{sal}=33.4 g l^{-1} and τ_{sal}=322 kyr to 59.2 °C, 29.3 g l^{-1} and 255 kyr, respectively. Overall, it can be concluded that the thermohaline dome continues to form beneath the discharge zone, slightly

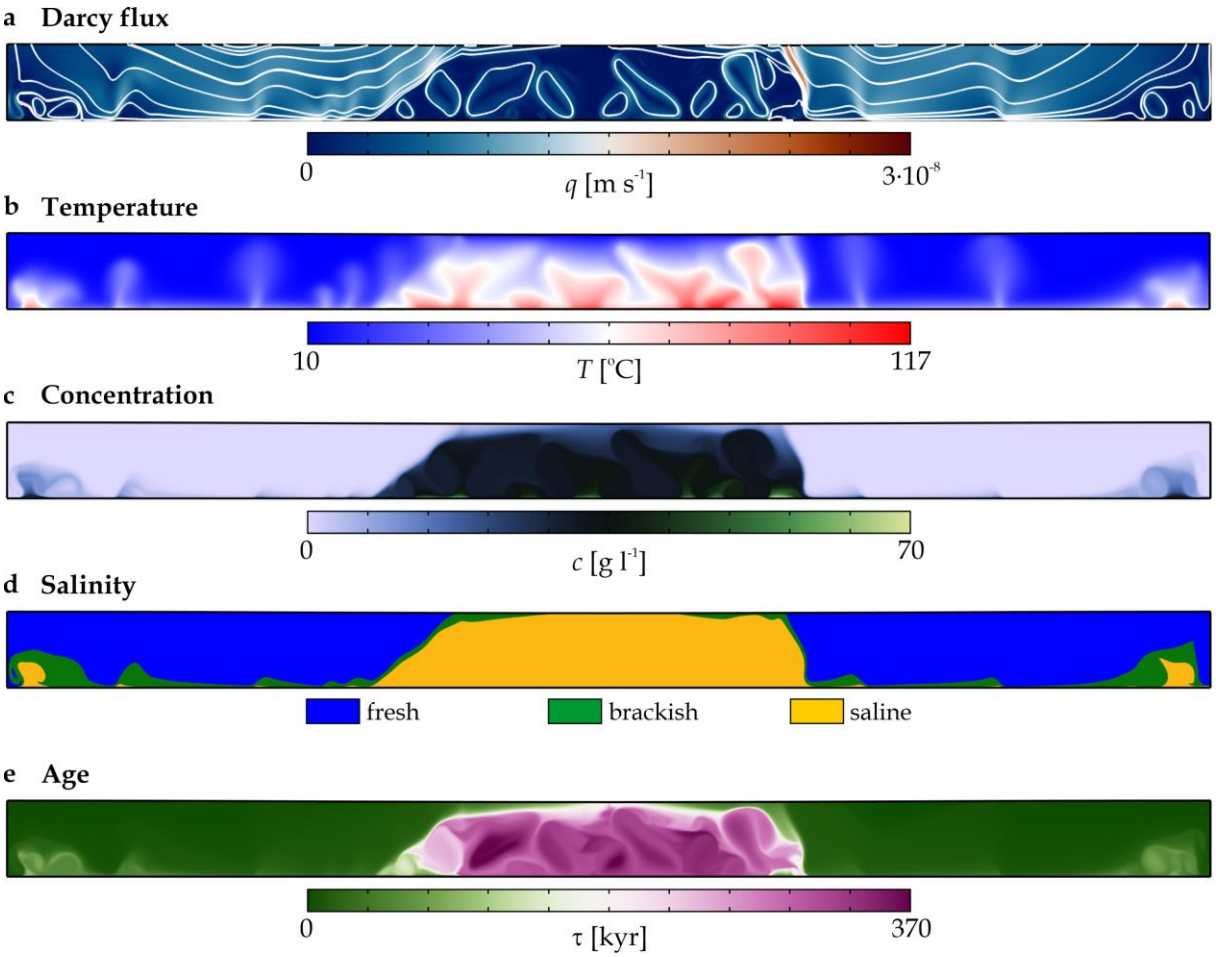

Figure S2 Snapshots of the (a) Darcy flux, (b) temperature, (c) salt concentration, (d) salinity zones and (e) water age at *t*=3.5 Myr after the initial state in the base model (Table 2) with doubled model domain. (a) Streamlines illustrate the flow direction. (d) Salinity zones: freshwater (blue), brackish water (green) and saline water (orange).

weakened in its quantitative character, but the features of topothermohaline convection are consistent with the phenomena in the unit basin presented in the paper.

S4 Effect of non-constant viscosity and bottom boundary condition in the BTK model

For simplicity and to save computational resources, the numerical calculations were performed at constant water viscosity. The present simulation illustrates the effect of temperature-, pressure- and concentration-dependent viscosity along the BTK section. The value of dynamic viscosity in the present hydrogeological model varied between $\mu=10^{-4}$ and $1.3\cdot10^{-3}$ Pa s and was mainly influenced by the temperature. In addition, an impermeable layer (k=0 m^2) of 1 km thickness was placed below the model domain, and the lower boundary conditions — which were the same as those described in Section 3.2.1 — were imposed at the bottom of this layer.

These two factors resulted in a more efficient reduction of salinity in the deep, confined reservoir because (1) the reduced viscosity due to high temperature led to more intense thermohaline convection and (2) salt was only transported by diffusion through the lower impermeable layer (Fig. S3). The lower salinity and reduced viscosity intensified the flow, thus slightly decreasing the water age. While no change in the maximum reservoir temperature was observed, its size was slightly decreased based on the model calculation. In contrast, in the regions near the discharge zone and below the Oligocene cover (HS6), a warming of a few degrees was observed, which is most likely a consequence of the more intense upwelling caused by the reduced viscosity. However, in terms of the basic characteristics of the BTK system, no substantial changes were found due to the two modified parameters (variable viscosity and modified lower boundary condition), topography-driven groundwater flow in the unconfined karst area and thermohaline convection in the confined reservoir being the dominant groundwater flow regimes. A reservoir with high geothermal potential has formed beneath the clayey cover containing saline/brackish and aged water, which can persist over geological time scales. We mention that BTK models were also calculated in which only one factor was changed (variable viscosity or bottom impermeable layer). Their solutions fell between the two models presented (Fig. 10 and Fig. S3) in terms of salt concentration. The presence of the bottom impermeable layer increased the water age in the confined reservoir, while the temperature-dependent viscosity slightly decreased the temperature.

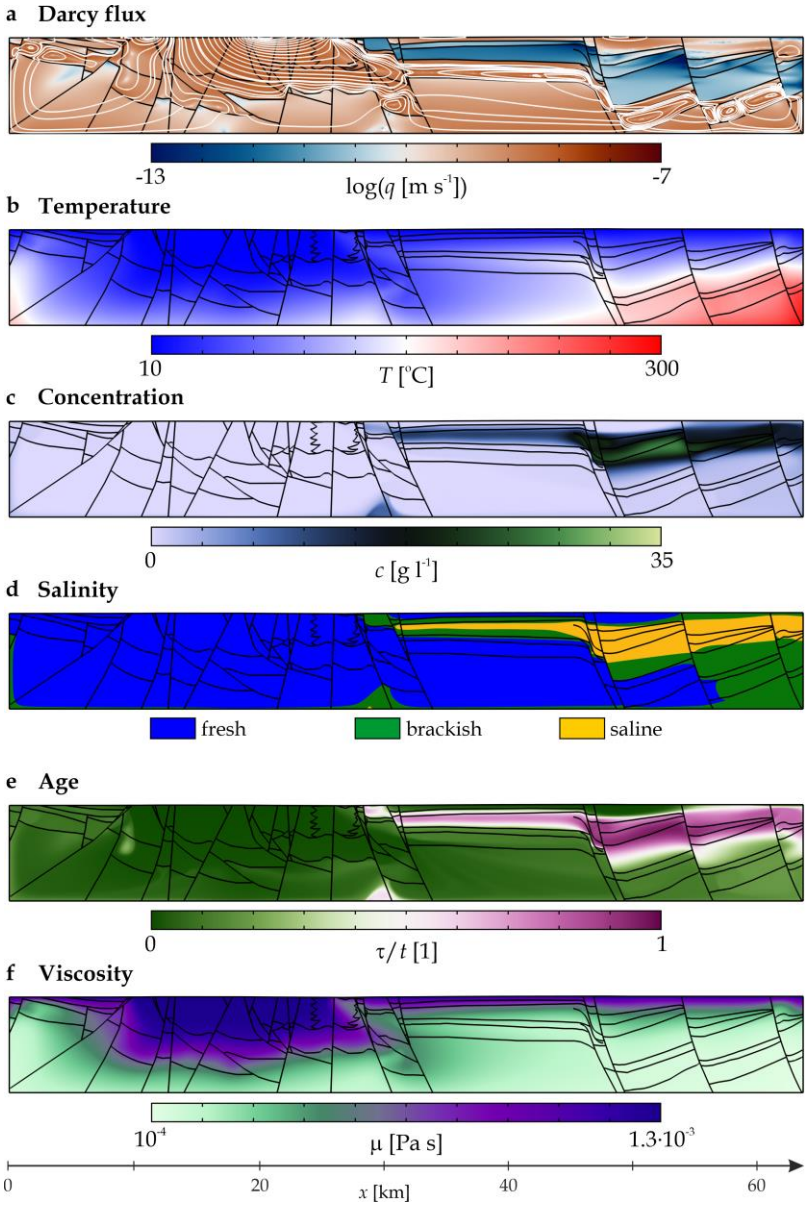

Figure S3 Solution of the topothermohaline convection in the Buda Thermal Karst system applying temperature-, pressure and concentration-dependent viscosity and a lower impermeable layer (not shown). Distributions of (a) the Darcy flux, (b) the temperature, (c) the salt concentration, (d) the salinity zones, (e) the water age and (f) the dynamic viscosity at 1 Myr. The direction of Darcy flux is illustrated with streamlines (white). The groundwater mean age, τ is normalized by the simulation time, *t*.

References

Magri, F.: Derivation of the coefficients of thermal expansion and compressibility for use in FEFLOW, White Papers III: DHI-WASY GmbH, Institute for Water Resource Planning and System Research, Berlin, pp. 13–23, https://hydrosoft.co.kr/sites/default/files/2024-04/Technical_Reference_FEFLOW_white_papers_vol3_ENG.pdf, 2009.

Kohfahl, C., Post, V.E.A., Hamann, E., Prommer, H., and Simmons, C.T.: Validity and slopes of the linear equation of state for natural brines in salt lake systems, Journal of Hydrology, 523, 190–195, http://dx.doi.org/10.1016/j.jhydrol.2015.01.054, 2015.

Easteal, A.J., Price, W.E., and Woolf, L.A.: Diaphragm cell for high-temperature diffusion measurements, Journal of the Chemical Society: Faraday Transactions 1, 85 (5), 1091–1097, https://doi.org/10.1039/F19898501091, 1989.

Galsa, A., Tóth, Á., Szijártó, M., Pedretti, D., and Mádl-Szőnyi, J.: Interaction of basin-scale topography- and salinity-driven groundwater flow in synthetic and real hydrogeological systems, Journal of Hydrology, 609, paper: 127695, https://doi.org/10.1016/j.jhydrol.2022.127695, 2022.